Higginsianins D and E, Cytotoxic Diterpenoids Produced by Colletotrichum higginsianum

Higginsianins D and E, Cytotoxic Diterpenoids Produced by Colletotrichum higginsianum

Marco Masi,[†] Alessio Cimmino,[†] Flora Salzano,[‡] Roberta Di Lecce,[†] Marcin Górecki,[±, §] Viola Calabrò,[‡] Gennaro Pescitelli,[±,*] and Antonio Evidente[†,*]

[†] Dipartimento di Scienze Chimiche, Università di Napoli "Federico II", Complesso Universitario Monte S. Angelo, Via Cintia 4, 80126 Napoli, Italy

[‡] Dipartimento di Biologia, Universitàdi Napoli Federico II, Complesso Universitario Monte Sant'Angelo, 80126 Napoli, Italy

[±]Dipartimento di Chimica e Chimica Industriale, Università di Pisa, Via Moruzzi 13, 56124 Pisa, Italy

[§]Institute of Organic Chemistry, Polish Academy of Sciences, Kasprzaka 44/52 St., 01-224Warsaw, Poland

ABSTRACT

Two new diterpenoids with tetrasubstituted 3-oxodihydrofuran substituents, named higginsianins D (**1**) and E (**2**), were isolated from the mycelium of the fungus *Colletotrichum higginsianum* grown in liquid culture. They were characterized as methyl 2-[6-hydroxy-5,8a-dimethyl-2-methylene-5-(4-methylpent-3-enyl)-decahydronaphthalen-1-ylmethyl]-4,5-dimethyl-3-oxo-2,3-dihydrofuran-2-carboxylate and its 21-epimer by using NMR, HRESIMS, and chemical methods. The relative configurations of higginsianins D and E, which did not afford crystals suitable for X-ray analysis, were determined by NOESY experiments and by comparison with NMR data of higginsianin B. The absolute configuration was established by comparison of experimental and calculated electronic circular dichroism data. The evaluation of **1** and **2** for antiproliferative activity against human A431 cells derived from epidermoid carcinoma and H1299 non-small-cell lung carcinoma cells revealed that 2 exhibited higher cytotoxic activity than 1, with an IC_{50} value of 1.0 μM against A431 cells. Remarkably, both **1** and **2** were almost ineffective against immortalized keratinocytes, used as a preneoplastic cell line model.

Colletotrichum is a fungal genus comprising a large number of endophytic, saprophytic, and plant pathogenic species. The latter are responsible for severe diseases to many crops, such as peaches, apples, pecans, and other hosts (Bernstein et al., 1995) and are considered some of the most harmful species in agriculture (Dean et al., 2012). However, the production of phytotoxic secondary metabolites potentially involved in plant pathogenesis by various *Colletotrichum* species is only partially explored. Among these, the phytotoxic metabolites named colletochlorins and colletorins, grouped in prenyl or diprenyl orsellinaldheyde derivatives, were isolated from *Colletotrichum tabacum* (synonym of *Colletotrichum nicotianae*), causing anthracnose in tobacco (García-Paión et al., 2003), and *Colletotrichum gloeosporioides*, a fungus proposed for biocontrol of *Ambrosia artemisiifolia* (Masi et al., 2018). The genus is also interesting for the capability of the species to produce a wide array of secondary metabolites possessing various biological properties (Kim et al., 2019). During a preliminary screening carried out on 89 strains belonging to many species of the genus *Colletotrichum* and aimed at finding novel bioactive metabolites, a strain of *Colletotrichum higginsianum*, belonging to the *Colletotrichum destructivum* species complex (Damm et al., 2014), was selected because its culture filtrate showed phytotoxic activity, while the EtOAc extract of its mycelium showed promising anticancer activity (Cimmino et al., 2016; Masi et al., 2017a). *C. higginsianum* is the causal agent of anthracnose leaf spot disease of several Brassicaceae crop species. This disease was also recently attributed to *Colletotrichum capsici*, causing anthracnose on bok choy (*Brassica chinensis*) in Malaysia (Mahmodi et al., 2013), or to *Colletotrichum truncatum*, found to cause severe anthracnose of Chinese flowering cabbage (*Brassica parachinensis*) (He et al., 2016).

From the culture filtrate of *C. higginsianum* a tetrasubstituted pyran-2-one and a tetrasubstituted dihydrobenzofuran, named colletochlorins E and F, respectively, were isolated together with the known chlorinated 3-diprenylorsellinaldehyde derivative colletochlorin A, 4-chlororcinol, and colletopyrone. Colletochlorin F and 4-chlororcinol showed significant activity on both weedy and parasitic plants, while colletochlorin A and colletopyrone showed modest activity

(Masi et al., 2017a). Subsequently, a new tetrasubstituted indolylidenepyrandione named colletopyrandione and a tetrasubstituted chroman- and a tetrasubstituted isochroman-3,5-diol, named colletochlorins G and H, respectively, were isolated from the culture filtrates of the same fungus. Only the colletopyrandione showed modest phytotoxicity (Masi et al, 2017b).

The bioguided purification of the EtOAc extract obtained from the mycelium of *C. higginsianum* led to the isolation of two new diterpenoids having an α-pyrone moiety located at C-4, named higginsianins A and B (Cimmino et al., 2016). In a preliminary evaluation against a six cancer cell panel together with three semisynthetic derivatives prepared from higginsianin A, both higginsianins A and B showed promising cytostatic rather than cytotoxic activity, while the activity of the derivatives provided the first structure−activity relationship correlations (Cimmino et al., 2016). Further investigations have been carried out on the anticancer activity of higginsianins A and B, and they have been demonstrated to induce cell cycle arrest in the S-phase associated with an increase of γH2AX positive nuclear foci, indicating the occurrence of DNA lesions (Sangermano et al., 2019).

The C*cl*A subunit of the COMPASS complex mediates the trimethylation of the lysine unit at position 4 of histone H3 (H3K4). Such epigenetic modification plays a critical role in regulating fungal growth, development, pathogenicity, and secondary metabolism in *C. higginsianum*. It was recently shown that a *C. higginsianum* strain with a deleted version of C*cl*A (Δ*cclA*) exhibited strongly reduced mycelial growth and spore germination as well as attenuated virulence on plants (Dallery et al. 2019a; Dallery et al. 2019b). The secondary metabolite profile of the Δ*cclA* mutant was different with respect to that of the wild type, with the presence of other metabolites belonging to the three different families of terpenoids, namely, the colletochlorins, higginsianins, and sclerosporide. From the liquid culture of the mutant ΔcclA were also isolated the new higginsianin C and 13-*epi*-higginsianin C, sclerosporide, colletorin D, and colletorin D acid (Dallery et al. 2019a; Dallery et al. 2019b).

Further investigation of the EtOAc extract obtained from the mycelium of C. higginsianum permitted isolation of two new metabolites structurally related to higginsianins, which were named higginsianins D and E, bearing an unusual trisubstituted 2-carboxymethyldihydrofuran-3-one moiety located at C-21. This article reports the isolation and the chemical and biological characterization of higginsianins D and E.

RESULTS AND DISCUSSION

The EtOAc extract of the *C. higginsianum* mycelium was further investigated. The chromatographic purification as reported in the Experimental Section led to the isolation of the known cytotoxic α-pyrone diterpenoids higginsianins A and B (**3** and **4**, Figure 1) (Cimmino et al., 2016; Sangermano et al., 2019) and the new natural products named higginsianins D (**1**) and E (**2**).

Preliminary investigation of the ^{1}H and ^{13}C NMR data of **1** and **2** showed that they share similar structures and are related to **4**, while their HRESIMS spectra showed the same sodium adduct ion from which the molecular formula of $C_{28}H_{42}O_5$ and eight hydrogen deficiencies were deduced. These findings were corroborated by the bands observed in the IR spectra for hydroxy, carbonyl, and olefinic groups (Nakanishi and Solomon, 1977), while the UV spectra showed bands typical of a conjugated carbonyl group (Pretsch et al., 2000). However, a noteworthy difference was observed for the moiety attached to C-4 when **1** and **2** were compared to **4**.

The ^{1}H NMR and COSY spectra17 of higginsianin D (**1**) (Table 1) showed a broad triplet (J = 7.1 Hz) and two coupled broad singlets, due to the protons of a trisubstituted olefinic and an exocyclic methylene group at δ 5.15 (H-13) and 4.69 and 4.51 (H_2C-19), the broad singlet of a proton of a secondary oxygenated carbon (HC-8) at δ 3.62, and the singlet of a methoxy group at δ 3.67. Furthermore, the signals for four vinylic methyl groups at δ 2.26, 1.68, 1.72, and 1.66 (Me-27, Me-26, Me-15, and Me-16), with the latter two coupled with H-13, were observed. Two other singlets, due to two tertiary aliphatic methyl groups (Me-18 and Me-17), resonated at δ 0.96 and 0.82. The C-8 proton coupled with the protons of the adjacent methylene group (H_2C-7), resonating

as a triplet of doublets (J = 14.3 and 2.2 Hz) at δ 2.15 and a multiplet at δ 1.94, being also coupled with the multiplets of the protons of the adjacent methylene group (H_2C-6) observed at δ 1.60 and 0.81. The H-10 multiplet at δ 1.59 coupled with protons of the adjacent methylene group (H_2C-1) that resonated as two multiplets at δ 1.60 and 1.33. These latter protons (H_2C-1) also coupled with the protons of the adjacent methylene group (H_2C-2) present as a triplet of doublets (J = 13.9 and 5.8 Hz) at δ 2.38 and a doublet of doublets of doublets (J = 13.9, 4.4, and 1.6 Hz) at δ 2.18. Furthermore, the multiplet of an aliphatic methine (HC-4), observed at δ 1.96, coupled with the protons of the adjacent methylene group (H_2C-20) resonating as a doublet of doublets (J = 14.6 and 10.8 Hz) and a multiplet at δ 2.53 and 2.12, respectively. Finally, the olefinic H-13 also coupled with the protons of the adjacent methylene group (H_2C-12) appearing as two multiplets at δ 1.95 and 1.61, which also coupled with the protons of the adjacent methylene group (H_2C-11) observed as a multiplet at δ 1.27. These findings suggested the presence of hexasubstituted decalin and 4-methylpent-3-en-1-yl moieties in **1** similar to those observed in **4**. In fact, the couplings observed in the HSQC spectrum (Berger and Braun, 2004) permitted assignment of the signals to the protonated carbons in the ^{13}C NMR (Table 1) spectrum and in particular those observed at δ 124.9, 110.4, 71.9, 52.7, 52.3, 39.9, 39.5, 38.1, 31.0, 25.6, 25.5, 22.7, 22.5, 18.8, 17.8, 14.8, and 5.9 to C-13, C-19, C-8, C-4, OMe, C-10, C-11, C-5, C-2, C-15, C-12, C-1, C-17, C-18, C-16, C-27, and C-26, respectively (Breitmaier and Voelter, 1987).

The ^{13}C NMR spectrum also showed signals typical of two carbonyls, two sp^3 and four sp^2 quaternary carbons, and an oxygenated tertiary carbon, which were assigned on the basis of couplings observed in the HMBC spectrum (Berger and Braun, 2004) (Table 1). In fact, C-22 coupled with Me-26, C-24 with Me-26 and Me-27, C-25 with H-20B and OMe, C-3 with H_2-20 and H-4, C-14 with Me-15 and Me-16, C-23 with Me-26 and Me-27, C-21 with H_2-20, C-9 with Me-17, and C-5 with Me-18. Thus, the signals at δ 198.8, 185.1, 166.1, 147.8, 131.8, 109.5, 89.9, 39.4, and 38.1 were assigned to C-22, C-24, C-25, C-3, C-14, C-23, C-21, C-9, and C-5, respectively (Breitmaier and Voelter, 1987). These finding supported the presence of a hexasubstituted decalin

119 moiety as in **4** but also showed the absence of the *α*-pyrone moiety that is replaced by a
120 tetrasubstituted 3-oxodihydrofuran-2-one moiety carrying a methoxycarbonyl group at C-21. Such a
121 ring structure is extremely rare among natural products. It has been previously found only in some
122 spiroditerpenoids where the dihydrofuran-2-one ring is part of the spiro moiety (Fujimoto et al.,
123 1996; Kwon et al., 2015).

124 Thus, the chemical shifts were assigned to all the protons and corresponding carbons as
125 reported in Table 1, and the structure of **1** was defined as methyl 2-[6-hydroxy-5,8adimethy l-2-
126 methylene-5-(4-methylpent-3-enyl)-decahydronaphthalen-1-ylmethyl]-4,5-dimethyl-3-oxo-2,3-
127 dihydrofuran-2-carboxylate. The structure assigned to **1** was confirmed by the HMBC couplings
128 shown in Table 1 and its HRESIMS data. The latter showed the sodiated adduct and protonated
129 dimers $[2M + Na]^+$ and $[2M + H]^+$, the sodium adduct $[M + Na]^+$, and protonated $[M + H]^+$ ions at
130 *m/z* 939, 917, 481, and 459.3129, respectively.

131 Higginsianin E (**2**) has the same molecular formula as **1** and showed similar IR, UV, and ^1H
132 and ^{13}C NMR spectra. In particular, the ^1H NMR spectra of **1** and **2** differed with respect to the
133 shielded (Δδ 0.33) and deshielded (Δδ 0.42) shifts of the C-20 methylene protons. These results
134 suggested that higginsianin E (**2**) is a diastereomer of **1**, in particular, its epimer at C-21.

135 The relative configurations of **1** and **2** were deduced from their NOESY data (Table 2)
136 (Berger and Braun, 2004). In particular, significant crosspeaks were observed between H-4 and Me-
137 18, H-8 and Me-17, and H-7A, Me-17 and Me-18, confirming in both isomers the same relative
138 configuration at C-4, with H-4 oriented equatorial and cis to Me-18.

139 To definitely confirm the unusual structure of the dihydrofuran-3-one moiety, we performed
140 NMR calculations using density functional theory (DFT) with the gaugeindependent atomic orbital
141 (GIAO) method. Because of the pronounced conformational flexibility of **1** and **2**, the structures
142 employed for NMR calculations were cut at the C-11/C-12 bond; that is, the chain attached at C-9
143 was replaced by a methyl group. Moreover, a computational protocol was employed purposely
144 developed for the prediction of ^{13}C NMR chemical shifts of flexible compounds (Hehre et al.,

2019). The protocol consists of NMR calculations run at the ωB97X-D/6-31G(d) level with an empirical chemical shift correction; the input structures are generated with a sequence of steps with final ωB97X-V/6-311+G(2df,2p)//ωB97X-D/6-31G(d) energy estimation and geometry optimization. The protocol leads usually to overall rms (root-mean-square) errors below 2 ppm between experimental and calculated ^{13}C chemical shifts (Hehre et al., 2019). In the current case, the protocol produced a set of ^{13}C signals in good agreement with the experimental spectra for both **1** and **2**. Focusing only on the dihydrofuran-3-one moiety the rms error was 1.75 ppm for (21*S*)-1 and 1.85 ppm for (21*R*)-2 (see Supporting Information). When the two isomeric structures were switched, the rms errors were, however, highly similar (1.7 and 1.9 ppm, respectively). Thus, NMR calculations confirmed the structures proposed for **1** and **2**, but they were not sufficient to distinguish the configuration at C-21.

This latter piece of information, together with the absolute configuration of **1** and **2**, could eventually be obtained from experimental and calculated ECD data. The experimental ECD spectra of **1** and **2** measured in MeCN were almost mirror images over the measured range (Figure 2 vs Figure 3, bottom panels, solid traces), while the corresponding absorption UV spectra were almost superimposable (Figures 2 and Figure 3, top panels). This simple fact itself reinforce the hypothesis that higginsianins D and E have opposite configurations at C-21, which is the center of chirality closest to the main chromophore, namely, the substituted enone included in the dihydrofuran-3-one ring. To simulate the ECD spectra (Pescitelli and Bruhn, 2016; Superchi et al., 2018), low-energy structures found during NMR calculations were reoptimized at the ωB97X-D/6-311+G(d,p)/PCM level and employed as input in time-dependent DFT calculations run at the ωB97X-D/def2-TZVP/PCM level, including in both cases a polarizable continuum solvent model for MeCN. Despite the presence of several low-energy minima, the final Boltzmann-averaged UV and ECD spectra agreed well with the experimental ones (Figures 2 and 3, solid traces vs dotted traces). We rely in particular on the UV and ECD bands centered at 270 nm, due to the enone π–π* transition, which is red-shifted by the presence of substituents on the enone system, thus obscuring the

otherwise diagnostic n–π* transition (Xue et al., 2012; Yang et al., 2012). The absolute configurations of the new compounds may be assigned as (4*R*,5*R*,8*R*,9*S*,10*R*,21*S*) for higginsianin D (**1**) and (4*R*,5*R*,8*R*,9*S*,10*R*,21*R*) for higginsianin E (**2**), respectively.

To summarize, two new diterpenoid dihydrofuran-3-ones, named higginsianins D (**1**) and E (**2**), were isolated from the mycelium of the fungus *C. higginsianum* grown in liquid culture. Their structures, including relative and absolute configurations, were fully elucidated using NMR techniques and experimental and calculated ECD. Obviously, their structures resemble those of the diterpenoid *α*-pyrones higginsianin A and B (**3** and **4**) previously isolated from the same fungus, subglutinols previously isolated from *Fusarium subglutinans* (Lee et al., 1995), higginsianin C and 13-*epi*-higginsianin C produced by another strain of *C. higginsianum* (Dallery et al., 2019b), and the diperpenoid BR-050 previously isolated from *Torrubiella luterostrata* (Pittayakhajonwut et al., 2009). Although a tetrasubstituted 3-oxodihydrofuran-2-one bearing a methoxycarbonyl group has not been found in nature, a similar structure has been synthesized (Arimoto et al., 1994).

The evaluation of the in vitro cytotoxicity of higginsianins D and E was performed by MTT assays in A431 and H1299 carcinoma cells as well as in HaCaT immortalized keratinocytes, used as a preneoplastic cell line model. The experiments with the new higginsianins were performed in parallel with the previously described higginsianin B as a positive control (Sangermano et al., 2019).

After 24 h of treatment, HaCaT cell viability was significantly reduced by higginsianin E, 40% at 1 μM and 37% at 10 μM, while higginsianin D had no effect. A moderate but significant reduction of cell viability was observed after 48h of incubation with a concentration of 10 μM higginsianin D or E. Interestingly, however, HaCaT cells fully recover after 72 h of treatment despite the presence of higginsianin E or D (Figure 4). In H1299, a similar effect was observed with higginsianin D at both concentrations, while higginsianin E caused 22% (at 1 μM) and 26% (at 10 μM) reduction after 72 h of treatment. A431 cell viability, instead, was strongly affected by both higginsianins in a time- and dose-dependent manner, and the IC_{50} of higginsianin E was 1 μM after

72 h of incubation (Figure 4). It is important to take into consideration that, unlike higginsianin B, higginsianin E showed no toxicity in HaCaT cells, at the same experimental conditions.

EXPERIMENTAL SECTION

General Experimental Procedures. Optical rotations were measured in a MeOH solution on a Jasco P-1010 digital polarimeter; IR spectra were recorded as a glassy film on a PerkinElmer Spectrum One FT-IR spectrometer, and UV spectra were recorded in MeOH solution on a PerkinElmer Lambda 25 UV/vis spectrophotometer. ECD spectra were recorded with a Jasco J-715 spectropolarimeter, on solutions of 3.3 mM in CH_3CN and using a quartz cell with a 0.01 cm path length. ECD measurement parameters were the following: scan speed 100 nm/min; time constant 0.5 s; bandwidth 1 nm; 4 accumulations. ^{1}H and ^{13}C NMR spectra were recorded at 400 and 100 MHz, respectively, in $CDCl_3$ on a Bruker spectrometer. The same solvent was used as an internal standard. Carbon multiplicities were determined by DEPT spectra (Berger and Braun, 2004). DEPT, COSY-45, HSQC, HMBC, and NOESY experiments (Berger and Braun, 2004) were performed using Bruker microprograms. HRESI and ESI mass spectra and liquid chromatography (LC)/MS analyses were performed using the LC/MS TOF system Agilent 6230B, HPLC 1260 Infinity. The HPLC separations were performed with a Phenomenex LUNA (C_{18} (2) 5 μ 150 × 4.6 mm). Analytical and preparative TLC were performed on silica gel plates (Merck, Kieselgel 60, F_{254}, 0.25 and 0.5 mm, respectively) or on reverse-phase (Whatman, KC18 F_{254}, 0.20 mm) plates; the compounds were visualized by exposure to UV light and/or iodine vapors and/or by spraying first with 10% H_2SO_4 in MeOH and then with 5% phosphomolybdic acid in EtOH, followed by heating at 110 °C for 10 min. CC: silica gel (Merck, Kieselgel 60, 0.063−0.200 mm).

Fungal Strain. The *C. higginsianum* isolate used in this study is IMI 349063 (CABI Culture Collection), as previously described (Cimmino et al., 2016).

Production, Extraction and Purification of Fungal Metabolites. The strain of *C. higginsianum* was grown in M1-D as previously reported (Cimmino et al., 2016). The harvested mycelium was lyophilized (14.5 g from 4.1 L of culture filtrate) and macerated with EtOAc (3 × 1 L) for 24 h at room temperature in the dark. The organic extracts were combined, dried with anhydrous Na_2SO_4, and evaporated under reduced pressure, yielding a brown oil residue (1.8 g). This oil was purified by CC eluted with $CHCl_3$–*i*-PrOH (97:3), yielding 10 groups of homogeneous fractions. The residue of the fourth fraction (234.5 mg) was purified by CC eluted with *n*-hexane–acetone (7:3), yielding six groups of homogeneous fractions. The residue (15.8 mg) of the third fraction of the latter column was purified on TLC eluted with *n*-hexane–EtOAc (7:3), affording two homogeneous amorphous solids, higginsianin D (**1**, 2.7 mg, R_f 0.36) and higginsianin E (**2**, 3.7 mg, R_f 0.39). The residue of the sixth fraction (65.1 mg) of the first column was crystallized using EtOAc–*n*-hexane (1:1), obtaining higginsianin A (**3**, 39.9 mg, R*f* 0.80) as white crystals. The eighth fraction of the first column was obtained as a homogeneous solid and identified as higginsianin B (**4**, 84.6 mg, R_f 0.50).

*Higginsianin D (**1**), Methyl 2-[6-Hydroxy-5,8a-dimethyl-2-methylene-5-(4-methylpent-3-enyl)decahydronaphthalen-1-ylmethyl]-4,5-dimethyl-3-oxo-2,3-dihydrofuran-2-carboxylate*: amorphous solid, $[\alpha]^{25}_D$ −34 (*c* 0.2); IR ν_{max} 3714, 1731, 1706, 1632, 1226 cm^{-1}; UV λ_{max} nm (log ε) 276 (3.6); ^1H and ^{13}C NMR see Table 1; HRESIMS (+) *m/z* 939 $[2M + Na]^+$, 917 $[2M + H]^+$, 481 $[M + Na]^+$, 459.3129 [calcd for $C_{28}H_{43}O_5$ 459.3111, $M + H]^+$.

*Higginsianin E (**2**), Methyl 2-[6-Hydroxy-5,8a-dimethyl-2-methylene-5-(4-methylpent-3-enyl)decahydronaphthalen-1-ylmethyl]-4,5-dimethyl-3-oxo-2,3-dihydrofuran-2-carboxylate*: amorphous solid, $[\alpha]^{25}_D$ +62 (*c* 0.2); IR ν_{max} 3710, 1748, 1706, 1630, 1205 cm^{-1}; UV λ_{max} nm (log ε) 275 (3.6); ^1H and ^{13}C NMR see Table 1; HRESIMS (+) *m/z* 939 $[2M + Na]^+$, 917 $[2M + H]^+$, 481 $[M + Na]^+$, 459.3130 [calcd for $C_{28}H_{43}O_5$ 459.3111, $M + H]^+$.

Cell Culture and Reagents. HaCaT, spontaneously immortalized keratinocytes from adult skin, were purchased from Service Cell Line and cultured as described (Amoresano et al., 2010). Human non-small-cell lung carcinoma cells H1299 (CRL-5803) and human epidermoid carcinoma cells A431 (ATCC-CRL1555) were from American Type Culture Collection (ATCC). According to the p53 compendium database (http://p53.fr/tp53-database/the-tp53-cell-linecompendium), HaCaT cells contain mutant p53 (H179Y/R282W), H1299 are p53 null, while A431 contain only one p53 mutated allele (R273H). All mentioned cell lines were cultured in Dulbecco's modified Eagle's medium (DMEM) supplemented with 10% fetal bovine serum (FBS) at 37 °C in a humidified atmosphere of 5% CO_2. All cell lines were routinely tested for mycoplasma contamination and were not infected.

Determination of the IC_{50} Growth Inhibitory Concentrations In Vitro. The MTT colorimetric assay was performed as previously described (Montano et al., 2019). Briefly, 2×10^4 cells were seeded on 24-well plates and exposed to increasing concentrations of either 1 or 10 μM higginsianins B, D, or E for 24, 48, and 72 h. MTT/DMEM without phenol red (0.5 mg/mL) was added to the wells and incubated for 3 h at 37 °C in a humidified atmosphere. The reaction was stopped by the removal of the supernatant, followed by dissolving the formazan product in acidic isopropanol. Optical density was measured with an ELISA reader (Bio-Rad) in a dual-wavelength mode (570 and 630 nm) filter using an iMark microplate reader (Bio-Rad) and calculated as follows: Absorbance (570 nm) − Absorbance (630 nm). Each experiment was performed in quadruplicate, in three independent experiments. The cell viability was calculated as (Absorbance of test sample)/(Absorbance of control).

Statistical analyses were carried out using the GraphPad Prism 8 software. Data were represented as the mean ± standard deviation and analyzed for statistical significance using ordinary one-way analysis of variance (ANOVA) and multiple comparisons. For all tests, $P < 0.5$ was considered to indicate a statistically significant difference.

Computational Methods. Molecular mechanics, Hartree−Fock (HF), and density functional theory (DFT) calculations were run with Spartan'18 (Wavefunction, Inc., Irvine, CA, 2018), with standard parameters and convergence criteria. DFT and TDDFT calculations were run with Gaussian16 (Frisch et al., 2016) with default grids and convergence criteria. All calculations were run on truncated models of **1** and **2** that were cut at the C-11/C-12 bond, that is, with the chain attached at C-9 replaced by a methyl group.

For NMR calculations, the conformers obtained by a conformational search run with the Monte Carlo algorithm using the Merck molecular force field (MMFF) were geometry-optimized at the HF/3-21G level, screened by single-point calculations at the ωB97X-D/6-31G(d) level, and geometry-optimized at the same level. Final energies and populations were estimated at the ωB97X-V/6-311+G(2df,2p) level, according to the procedure described by Hehre et al., 2019. The procedure afforded 20 energy minima for (21*S*)-**1** and 21 minima for (21*R*)-**2** within the final energy threshold (10 kJ/mol at the ωB97X-D/6-31G(d) level). ^{13}C NMR chemical shifts were then calculated with the GIAO method at the ωB97X-D/6-31G(d) level. Finally, an empirical correction was applied depending on the number of bonds to the carbon and on the bond lengths (Hehre et al., 2019).

For ECD calculations, the sets of low-energy minima found as described above were reoptimized at the ωB97X-D/6-311+G(d,p)/PCM level including the IEF-PCM continuum solvent model for MeCN and rechecked for duplicates and energy threshold. This led to 14 conformers for (21*S*)-**1** and 15 conformers for (21*R*)-**2**, which were used as input structures for TDDFT calculations run at the ωB97X-D/def2-TZVP/PCM level, including 36 excited states (roots) in each case. Other functionals (CAM-B3LYP and B3LYP) were checked for consistency on selected structures. Average ECD spectra were computed by weighting component ECD spectra with Boltzmann factors at 300 K estimated from DFT internal energies. ECD spectra were generated using the program SpecDis (Bruhn et al., 2017), using dipole-length rotational strengths; the difference from dipole-velocity values was negligible in all cases.

ASSOCIATED CONTENT

Supporting Information

The Supporting Information is available free of charge at https://pubs.acs.org/doi/10.1021/acs.jnatprod.9b01161.

Additional spectra of 1 and 2, low-energy DFT structures, and details on NMR calculations (PDF)

AUTHOR INFORMATION

Corresponding author

Gennaro Pescitelli − Dipartimento di Chimica e Chimica Industriale, Universitàdi Pisa, 56124 Pisa, Italy; orcid.org/0000-0002-0869-5076; Phone: +39 050 2219339; Email: gennaro.pescitelli@unipi.it

Antonio Evidente − Dipartimento di Scienze Chimiche, Università di Napoli Federico II, Complesso Universitario Monte Sant'Angelo, 80126 Napoli, Italy; orcid.org/0000-0001-9110-1656; Phone: +39 081 2539178; Email: evidente@unina.it

Authors

Marco Masi − Dipartimento di Scienze Chimiche, Università di Napoli Federico II, Complesso Universitario Monte Sant'Angelo, 80126 Napoli, Italy; orcid.org/0000-0003-0609-8902

Alessio Cimmino − Dipartimento di Scienze Chimiche, Università di Napoli Federico II, Complesso Universitario Monte Sant'Angelo, 80126 Napoli, Italy; orcid.org/0000-0002-1551-4237

Flora Salzano − Dipartimento di Biologia, Universitàdi Napoli Federico II, Complesso Universitario Monte Sant'Angelo, 80126 Napoli, Italy

Roberta Di Lecce − Dipartimento di Scienze Chimiche, Università di Napoli Federico II, Complesso Universitario Monte Sant'Angelo, 80126 Napoli, Italy

Marcin Górecki − Dipartimento di Chimica e Chimica Industriale, Università di Pisa, 56124 Pisa, Italy; Institute of Organic Chemistry, Polish Academy of Sciences, 01-224 Warsaw, Poland; orcid.org/0000-0001-7472-3875

Viola Calabrò− Dipartimento di Biologia, Universitàdi Napoli Federico II, Complesso Universitario Monte Sant'Angelo, 80126 Napoli, Italy; orcid.org/0000-0002-6508-8889

Complete contact information is available at: https://pubs.acs.org/10.1021/acs.jnatprod.9b01161

Notes

The authors declare no competing financial interest.

ACKNOWLEDGMENTS

This research was funded by Programme STAR 2017, financially supported by UniNA and Compagnia di San Paolo grant number E62F16001250003. The authors thank Dr. Riccardo Baroncelli, University of Salamanca, Salamanca, Spain, for the strain of *C. higginsianum* and Dr. Maurizio Vurro, Maria Chiara Zonno, and Angela Boari, Istituto di Scienze delle Produzioni Alimentari, CNR, Bari Italy, for the culture filtrates. M.G. thanks the program Bekker of the Polish National Agency for Academic Exchange. G.P. acknowledges the CINECA award under the ISCRA initiative for the availability of high-performance computing resources and support. A.E. is associated with the Istituto di Chimica Biomolecolare del CNR, Pozzuoli, Italy.

REFERENCES

Bernstein, B.; Zehr, E. I.; Dean, R. A.; Shabi, E. Plant Dis. 1995, 79, 478−482.

Dean, R.; Van Kan, J. A. L.; Pretorius, Z. A.; Hammond-Kosack, K. E.; Di Pietro, A.; Spanu, P. D.; Rudd, J. J.; Dickman, M.; Kahmann, R.; Ellis, J.; Foster, G. D. Mol. Plant Pathol. 2012, 13, 414−430.

García-Paión, C. M.; Collado, I. G. Nat. Prod. Rep. 2003, 20, 426−431.

348 Masi, M.; Zonno, M. C.; Cimmino, A.; Reveglia, P.; Berestetskiy, A.; Boari, A.; Vurro, M.;
349 Evidente, A. Nat. Prod. Res. 2018, 32, 1537− 1547.
350 Kim, J. W.; Shim, S. H. Arch. Pharmacal Res. 2019, 42, 735−753.
351 Damm, U.; O'Connell, R. J.; Groenewald, Z. J. P.; Crous, W. Stud. Mycol. 2014, 79, 49−84.
352 Cimmino, A.; Mathieu, V.; Masi, M.; Baroncelli, R.; Boari, A.; Pescitelli, G.; Ferderin, M.; Lisy,
353 R.; Evidente, M.; Tuzi, A.; Zonno, M. C. J. Nat. Prod. 2016, 79, 116−125.
354 Masi, M.; Cimmino, A.; Boari, A.; Tuzi, A.; Zonno, M. C.; Baroncelli, R.; Vurro, M.; Evidente, A.
355 J. Agric. Food Chem. 2017, 65, 1124−1130.
356 Mahmodi, F.; Kadir, J. B.; Wong, M. Y.; Nasehi, A.; Soleimani, N.; Puteh, A. Plant Dis. 2013, 97,
357 687−687.
358 He, Y.; Chen, Q.; Shu, C.; Yang, M.; Zhou, E. Trop. Plant Pathol. 2016, 4, 183−192.
359 Masi, M.; Cimmino, A.; Boari, A.; Zonno, M. C.; Górecki, M.; Pescitelli, G.; Tuzi, A.; Vurro, M.;
360 Evidente, A. Tetrahedron 2017, 73, 6644−6650.
361 Sangermano, F.; Masi, M.; Vivo, M.; Ravindra, P.; Cimmino, A.; Pollice, A.; Evidente, A.;
362 Calabrò, V. Toxicol. In Vitro 2019, 61, 104614.
363 Dallery, J. F.; Adelin, É.; Le Goff, G.; Pigné, S.; Auger, A.; Ouazzani, J.; O'Connell, R. J. Mol.
364 Plant Pathol. 2019, 20, 831−842.
365 Dallery, J. F.; Le Goff, G.; Adelin, E.; Iorga, B. I.; Pigné, S.; O'Connell, R. J.; Ouazzani, J. J. Nat.
366 Prod. 2019, 82, 813−822.
367 Nakanishi, K.; Solomon, P. H. Infrared Absorption Spectroscopy, 2nd ed.; Holden Day: Oakland,
368 1977; pp 17−44.
369 Pretsch, E.; Bühlmann, P.; Affolter, C. Structure Determination of Organic Compounds − Tables of
370 Spectral Data, 3rd ed.; Springer- Verlag: Berlin, 2000; pp 161−243.
371 Berger, S.; Braun, S. 200 and More Basic NMR Experiments: a Practical Course, 1st ed.; Wiley-
372 VCH: Weinheim, 2004.
373 Breitmaier, E.; Voelter, W. Carbon-13 NMR Spectroscopy; VCH: Weinheim, 1987; pp 183−280.

374 Fujimoto, H.; Negishi, E.; Yamaguchi, K.; Nishi, N.; Yamazaki, M. Chem. Pharm. Bull. 1996, 44,
375 1843−1848.
376 Kwon, J.; Seo, Y. H.; Lee, J.-E.; Seo, E.-K.; Li, S.; Guo, Y.; Hong, S.-B.; Park, S.-Y.; Lee, D. J.
377 Nat. Prod. 2015, 78, 2572−2579.
378 Hehre, W.; Klunzinger, P.; Deppmeier, B.; Driessen, A.; Uchida, N.; Hashimoto, M.; Fukushi, E.;
379 Takata, Y. J. Nat. Prod. 2019, 82, 2299−2306.
380 Pescitelli, G.; Bruhn, T. Chirality 2016, 28, 466−474.
381 Superchi, S.; Scafato, P.; Górecki, M.; Pescitelli, G. Curr. Med. Chem. 2018, 25, 287−320.
382 Xue, M.; Zhang, Q.; Gao, J.- M.; Li, H.; Tian, J.- M.; Pescitelli, G. Chirality 2012, 24, 668−674.
383 Yang, S.- X.; Gao, J.- M.; Laatsch, H.; Tian, J.- M.; Pescitelli, G. Chirality 2012, 24, 621−627.
384 Lee, J. C.; Lobkovsky, E.; Pliam, N. B.; Strobel, G.; Clardy, J. J. J. Org. Chem. 1995, 60,
385 7076−7077.
386 Pittayakhajonwut, P.; Usuwan, A.; Intaraudom, C.; Khoyaiklang, P.; Supothina, S. Tetrahedron
387 2009, 65, 6069−6073.
388 Arimoto, H.; Ohba, S.; Nishiyama, S.; Yamamura, S. Tetrahedron Lett. 1994, 35, 4581−4584.
389 Amoresano, A.; Di Costanzo, A.; Leo, G.; Di Cunto, F.; La Mantia, G.; Guerrini, L.; Calabrò, V. J.
390 Proteome Res. 2010, 4, 2042−2048.
391 Montano, E.; Vivo, M.; Guarino, A. M.; di Martino, O.; Di Luccia, B.; Calabrò, V.; Caserta, S.;
392 Pollice, A. Pharmaceuticals 2019, 12, 72.
393 Frisch, M. J.; Trucks, G. W.; Schlegel, H. B.; Scuseria, G. E.; Robb, M. A.; Cheeseman, J. R.;
394 Scalmani, G.; Barone, V.; Petersson, G. A.; Nakatsuji, H.; Li, X.; Caricato, M.; Marenich, A. V.;
395 Bloino, J.; Janesko, B. G.; Gomperts, R.; Mennucci, B.; Hratchian, H. P.; Ortiz, J. V.; Izmaylov,
396 A. F.; Sonnemberg, J. L.; Williams-Young, D.; Ding, F.; Lipparini, F.; Egidi, F.; Goings, J.;
397 Peng, B.; Petrone, A.; Henderson, T.; Ranasinghe, D.; Zakrzewski, V. G.; Gao, J.; Rega, N.;
398 Zheng, G.; Liang, W.; Hada, M.; Ehara, M.; Toyota, K.; Fukuda, R.; Hasegawa, J.; Ishida, M.;
399 Nakajima, T.; Honda, Y.; Kitao, O.; Nakai, H.; Vreven, T.; Throssell, K.; Montgomery, J. A., Jr.;

Peralta, J. E.; Ogliaro, F.; Bearpark, M.; Heyd, J. J.; Brothers, E.; Kudin, K. N.; Staroverov, V. N.; Keith, T. A.; Kobayashi, R.; Normand, J.; Raghavachari, K.; Rendell, A.; Burant, J. C.; Iyengar, S. S.; Tomasi, J.; Cossi, M.; Millam, J. M.; Klene, M.; Adamo, C.; Cammi, R.; Ochterski, J. W.; Martin, R. L.; Morokuma, K.; Farkas, O.; Foresman, J. B.; Fox, D. J. Gaussian 16, Revision A.03; Gaussian, Inc.: Wallingford, CT, 2016.

Bruhn, T.; Schaumlöffel, A.; Hemberger, Y.; Pescitelli, G. SpecDis Version 1.70; Berlin, Germany, 2017; https://specdissoftware.jimdo.com/.

Table 1. ^{1}H and ^{13}C NMR Data of Higginsianins D and E (1 and 2)[a,b]

	1			2		
position	δ_C[c]	δ_H (J in Hz)	HMBC	δ_C[c]	δ_H (J in Hz)	HMBC
1	22.7 CH_2	1.60, m	H-10	22.6 CH_2	1.62, m	H-10
		1.33, m			1.32, m	
2	31.0 CH_2	2.38, td (13.9, 5.8)	H-4, H-19B	31.5 CH_2	2.24, m	H-4, H_2-19
		2.18, ddd (13.9, 4.4, 1.6)			2.18, m	
3	147.8 C		H_2-20, H-4	148.5 C		H_2-20, H-4
4	52.7 CH	1.96, m	H_2-20, Me-18	52.3 CH	1.82, dd (9.9, 2.4)	H_2-19, Me-18, H-20B
5	38.1 C		Me-18	38.1 C		Me-18
6	28.1 CH_2	1.60, m	Me-18	28.4 CH_2	1.60, m	H-8, H-7A, Me-18
		0.81, m			0.81, m	
7	21.5 CH_2	2.15, td (14.3, 2.2)		25.7 CH_2	1.93, m	
		1.94, m			1.58, m	
8	71.9 CH	3.62, br s	Me-17	71.9 CH	3.61, br s	Me-17
9	39.4 C		Me-17	39.4 C		Me-17
10	39.9 CH	1.59, m	Me-18, Me-17	39.9 CH	1.59, m	Me-18, Me-17
11	39.5 CH_2	1.27, m (2H)	H-10, Me-17	39.5 CH_2	1.27, m (2H)	Me-17
12	25.5 CH_2	1.95, m		25.8 CH_2	1.93, m	
		1.61, m			1.58, m	
13	124.9 CH	5.15, br t (7.1)	Me-15, Me-16	125.0 CH	5.11, br t (7.0)	Me-15, Me-16
14	131.8 C		Me-15, Me-16	131.8 C		Me-15, Me-16
15	25.6 CH_3	1.72, br s[d]	Me-16	25.4 CH_3	1.69, br s[e]	Me-16
16	17.8 CH_3	1.66, br s[d]	Me-15	17.8 CH_3	1.62, br s[e]	Me-15
17	22.5 CH_3	0.82, s		22.4 CH_3	0.81, s	H_2-11, H-10
18	18.8 CH_3	0.96, s	H-1	18.7 CH_3	0.96, s	H-1
19	110.4 CH_2	4.69, br s	H-4	110.6 CH_2	4.65, br s	H-4
		4.51, br s			4.34, br s	
20	31.4 CH_2	2.53, dd (14.6, 10.8)	H-4	32.2 CH_2	2.20, dd (14.2, 9.9)	H-4
		2.12, m			2.54, dd (14.2, 2.4)	
21	89.9 C		H_2-20	90.1 C		H_2-20
22	198.8 C		Me-26	198.3 C		Me-26
23	109.5 C		Me-26, Me-27	109.4 C		Me-26, Me-27
24	185.1 C		Me-26, Me-27	184.8 C		Me-26, Me-27
25	166.1 C		H-20B, OMe	166.4 C		H-20B, OMe
26	5.9 CH_3	1.68, s		5.8 CH_3	1.65, s	
27	14.8 CH_3	2.26, s		14.6 CH_3	2.24, s	
OMe	52.3 CH_3	3.67, s	H-20B	53.0 CH_3	3.73, s	

[a]The chemical shifts are in δ values (ppm) from TMS. [b]2D ^{1}H,^{1}H (COSY), ^{13}C, ^{1}H (HSQC) NMR experiments delineated the correlations of all protons and their corresponding carbons. [c]Multiplicities were assigned by the DEPT spectrum. [d,e]These signals could be reversed.

Table 2. NOESY Data of Higginsianins E and D (1 and 2)

1		2	
irradiated	observed	irradiated	observed
H-4	Me-18	H-4	Me-18
H-8	Me-17, H-7A	H-8	Me-17, H-7A
Me-17	Me-18	Me-17	Me-18
H-20A	H-20B	H-20A	H-20B

Figure Legend

Figure 1. Structures of higginsianins D and E (**1** and **2**) and higginsianins A and B (**3** and **4**).

Figure 2. UV−vis absorption (top) and ECD spectra (bottom) of higginsianin D (**1**) measured in acetonitrile (solid lines, 3.3 mM, 0.01 cm cell) compared with spectra calculated for (21*S*)-**1** at the ωB97XD/def2-TZVP/PCM level as a Boltzmann average of 14 conformers at 300 K (dotted lines). Calculated spectra were obtained as sums of Gaussian bands with 0.3 eV exponential half-width, red-shifted by 15 nm, no vertical scaling.

Figure 3. UV−vis absorption (top) and ECD spectra (bottom) of higginsianin E (**2**) measured in acetonitrile (solid lines, 3.3 mM, 0.01 cm cell) compared with spectra calculated for (21*R*)-**2** at the ωB97XD/def2-TZVP/PCM level as a Boltzmann average of 15 conformers at 300 K (dotted lines). Calculated spectra were obtained as sums of Gaussian bands with 0.3 eV exponential half-width, red-shifted by 15 nm, ECD spectrum scaled by a factor 1.5.

Figure 4. Effects of higginsianins D, E, and B on HaCaT cell viability. MTT assay of HaCaT cells incubated for 24, 48, and 72 h with higginsianins B, D, and E at 1 or 10 μM, as indicated. Data are expressed as absorbance and presented as mean ± SD of three independent experiments, each done in triplicate. Analysis of variance was performed by one-way Anova and multiple comparisons. *$P < 0.5$ when compared with the control.

Figure 1

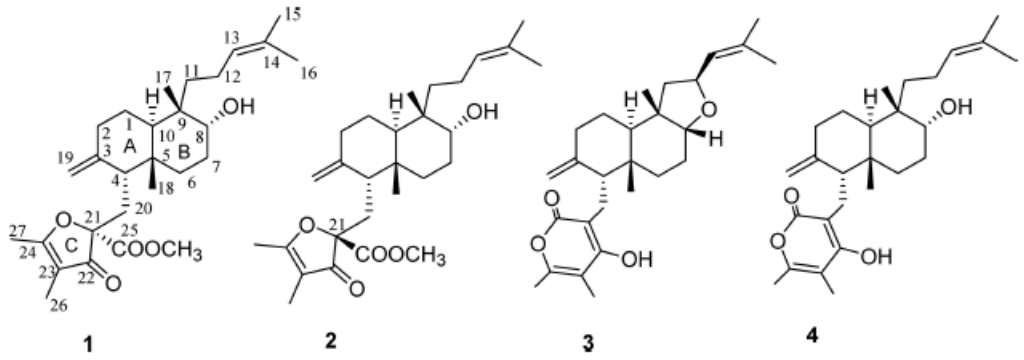

Figure 2

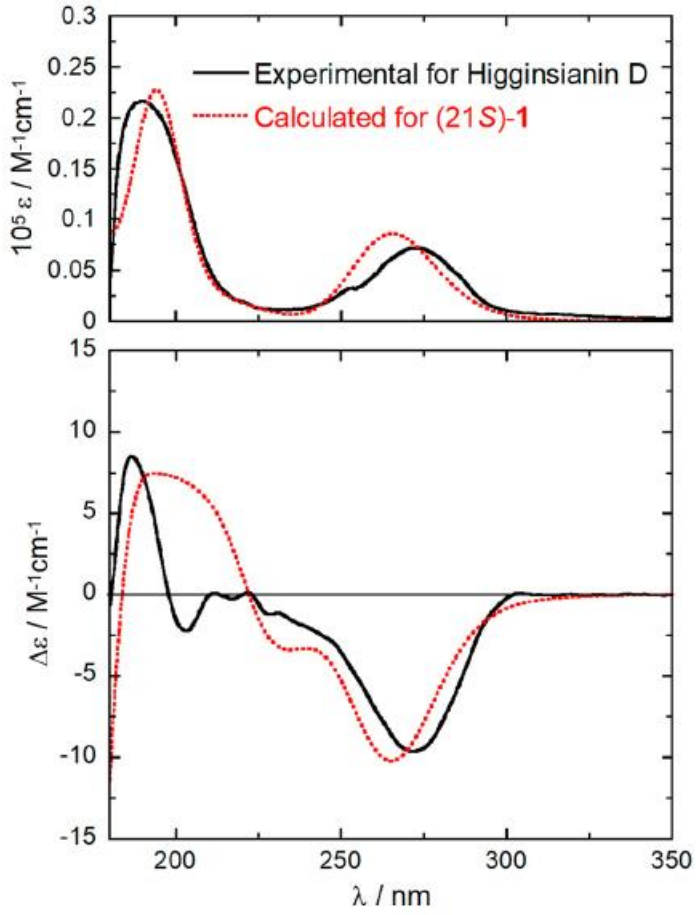

Figure 3

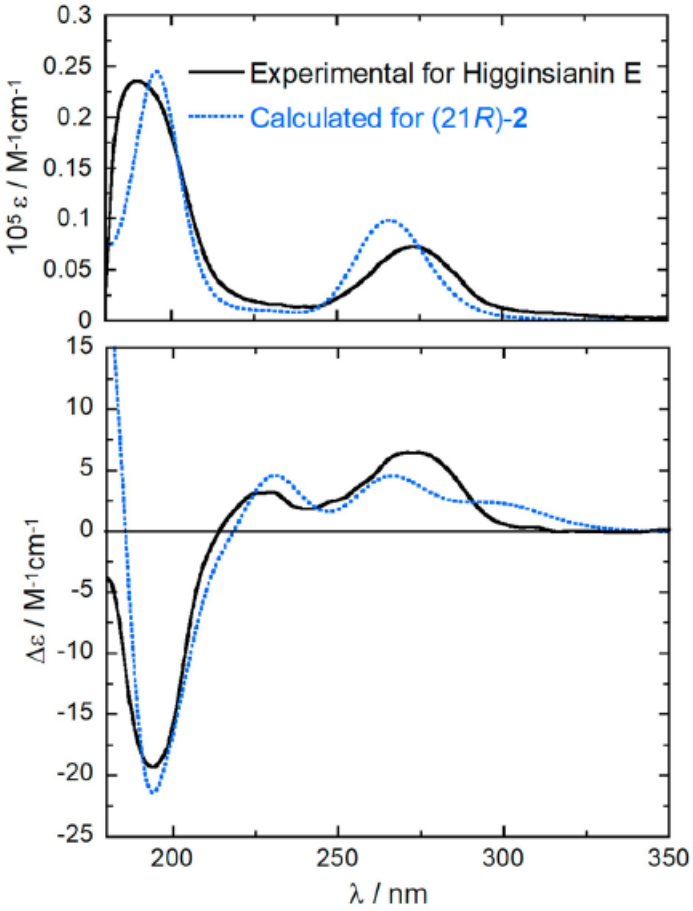
Experimental for Higginsianin E
Calculated for (21R)-2
$10^5\,\varepsilon$ / $M^{-1}cm^{-1}$
$\Delta\varepsilon$ / $M^{-1}cm^{-1}$
λ / nm
0.3
0.25
0.2
0.15
0.1
0.05
0
15
10
5
0
-5
-10
-15
-20
-25
200
250
300
350

480 **Figure 4**

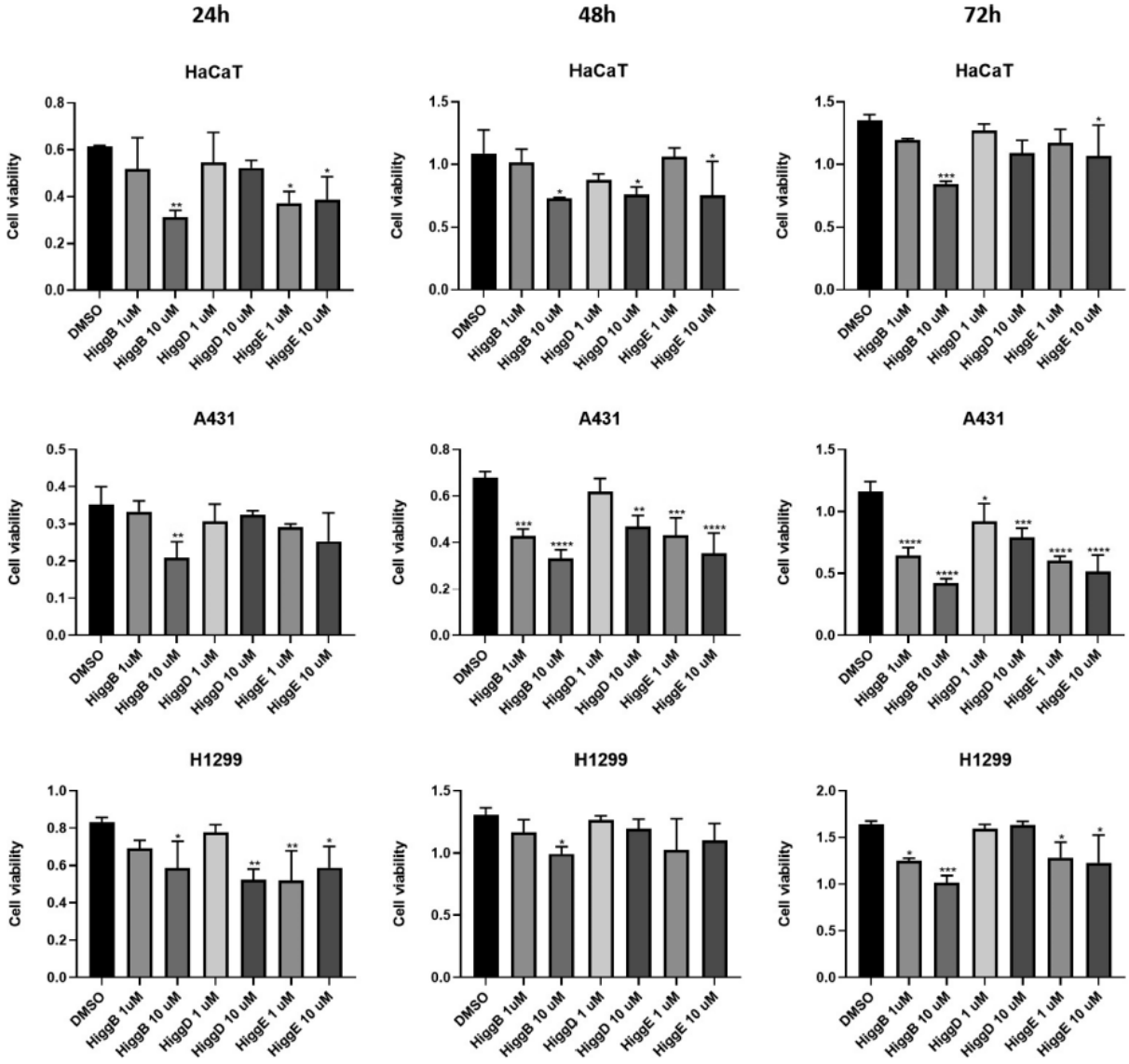

481

Table of Contents Graphics